PAPER

Physical modeling of the spreading of epigenetic modifications through transient DNA looping

IOP Publishing Journal of Physics A: Mathematical and Theoretical
J. Phys. A: Math. Theor. **52** (2019) 434001 (20pp) https://doi.org/10.1088/1751-8121/ab41d2

Physical modeling of the spreading of epigenetic modifications through transient DNA looping

Sarah H Sandholtz[1], Bruno G Beltran[2] and Andrew J Spakowitz[2,3,4,5,6]

[1] Department of Chemistry, Stanford University, Stanford, CA, 94305, United States of America
[2] Biophysics Program, Stanford University, Stanford, CA, 94305, United States of America
[3] Department of Chemical Engineering, Stanford University, Stanford, CA, 94305, United States of America
[4] Department of Materials Science and Engineering, Stanford University, Stanford, CA, 94305, United States of America
[5] Department of Applied Physics, Stanford University, Stanford, CA, 94305, United States of America

E-mail: ajspakow@stanford.edu

Received 11 February 2019, revised 26 August 2019
Accepted for publication 5 September 2019
Published 30 September 2019

Abstract

We utilize theoretical modeling to explore the physical mechanisms that govern the spreading of epigenetic modifications along chromosomal DNA. We focus on a particular modification, methylation of lysine 9 of histone H3 (H3K9), which is a representative and critical epigenetic mark that affects chromatin structure and gene expression. Our model captures transient loop formation in chromosomal DNA that enables distal segments to be in close spatial proximity and permits methyltransferase to confer methyl marks over a broad range of genomic distances. Using our exact results for the statistical behavior of a semiflexible polymer, we find the looping rate for a chromosomal segment based on a mean first-passage time process on a free-energy landscape. From this treatment, looping kinetics are predicted to be the rate-limiting process for methyl spreading at large genomic distances, which explains the considerable variability in the methyl profile at such scales. We then develop a 'phase diagram' for methylation spreading versus the methylation rate and the concentration of HP1, which we identify as a global regulator of the state of the chromosomal DNA.

Keywords: chromosomal dynamics, epigenetics, polymer physics

(Some figures may appear in colour only in the online journal)

[6] Author to whom any correspondence should be addressed.

1. Introduction

Epigenetics refers to variations in gene expression that are caused not by changes in the sequence of DNA basepairs but by chemical modifications to the chromosomal DNA and by post-translational modifications to DNA-packaging proteins. Epigenetic marks alter the spatial organization of the chromosome and the accessibility of genes to transcription factors, thereby affecting gene expression. Thus, cellular identity and behavior are not determined solely by the DNA sequence, and it is important to recognize that gene expression also depends on the physical organization of the DNA. Improving our understanding of gene expression therefore requires first gaining insight into the physical mechanisms that govern chromosome organization and the conferral of epigenetic marks.

Nucleosome core particles, which consist of DNA wrapped around a set of eight histone proteins, give chromosomal DNA its structure. Methylation and acetylation of the tails of these histone proteins are among the most important marks that drive changes in the local and global compaction of the chromatin fiber. For example, trimethylation of histone H3 lysine 9 (H3K9me3) is a critical epigenetic modification that interacts with heterochromatin protein 1 (HP1), which is required for the formation of heterochromatin [1]. When HP1α binds to H3K9 tails of adjacent nucleosomes [2–4], it oligomerizes, causing chromatin to condense [1, 5]. HP1α also interacts with the methyltransferase SuVar3-9 [6–8], which facilitates the conferral of methyl marks to neighboring histones. SuVar3-9 and HP1 coordinate their function throughout the process of conferral of methyl marks from parent to daughter cell through biophysical mechanisms that are currently not understood.

The coordination between SuVar3-9 and HP1 is inferred from experiments that attach an HP1 subunit to a genomic site and track the local spreading of H3K9me3 to neighboring nucleosomes [9]. Hodges and Crabtree [10] develop a kinetic model for the spreading of methyl marks through the interaction between methyltransferase and HP1α. This theoretical model provides a fundamental understanding of the dynamics and extent of spreading of the methylation profile based on spatial coordination of chromosomal segments. In this treatment, methyl marks spread to neighboring nucleosomes or to distal nucleosomes using a distance-dependent reaction rate.

Similarly, Erdel *et al* model loop-driven epigenetic spreading about a nucleation site. In their model, histone modifiers can spread epigenetic marks beyond the nearest neighbor according to the contact probability for two nucleosomes separated by a given length of DNA. They use experimental measurements of contact probabilities in human and Drosophila cells and find that their spreading model agrees with experimental results [11].

Foundational models demonstrate that cooperativity and long-range contacts are required to establish robust epigenetic domains [12, 13]. Additional modeling efforts incorporate the favorable interaction between nucleosomes with the same epigenetic state. For instance, Jost *et al* combine a copolymer model with an epigenetic regulation model and find that coupling between 1D epigenomic sequence and 3D compartmentalization is critical for long-range spreading of epigenetic marks and the formation of stable antagonistic epigenetic domains [14]. Similarly, Michieletto *et al* show that coupling between 3D folding of a semiflexible polymer and 1D epigenetic spreading leads to bistability and epigenetic memory [15]. While these models explain how the kinetics of the methyltransferase and the 3D organization of the chromatin would contribute to methyl spreading, they do not address the effect of transient DNA loops on the spreading process.

Various measurements of *in vivo* chromosomal dynamics demonstrate that chromosomal loci exhibit extremely slow dynamic behavior that can be characterized by significant viscoelastic resistance to their motion [16–21]. Previous work has demonstrated that DNA dynamics

play a significant role in the kinetics of looping events in *Escherichia coli*, as mediated by the Lac repressor protein [22, 23]. Chromosome capture experiments (e.g. Hi-C) [24–26] that map contact between genomically distant chromosomal loci display distinct patterns that correlate with epigenetic histone modifications, suggesting a connection between DNA looping and epigenetic regulation [15, 27–32]. The prominent plaid pattern in Hi-C contact maps indicates that DNA is organized into many distinct, self-associated domains. Several polymer-physics based models recapitulate such experimental observations of phase segregation in chromatin and reinforce the idea that the 3D chromatin structure and epigenetic profile are interrelated [28, 29, 31, 32]. Chromosomal dynamics are believed to play a critical role in the process of organizing the chromosomes into distinct territories that define the intra- and inter-chromosomal contacts [28, 33, 34]. The chromosomal organization is likely to exhibit considerable heterogeneity from cell to cell, and chromosomal changes throughout the cell cycle would further contribute to the heterogeneity of chromosomal contact maps [35] that are postulated to influence methyl-mark conferral [10].

In this manuscript, we present a theoretical model of the physical mechanisms that govern the spreading of epigenetic modifications through transient DNA looping. Our goal is to formulate our theory based on our current understanding of chromosomal dynamics [22, 23] and kinetics of the methyltransferase. Taking inspiration from the experimental measurements by Hathaway *et al* [9], we focus on a model where the chromosome is assumed to be uncondensed, which is a reasonable representation of the chromosome prior to cell differentiation. We utilize our exact results for the statistical behavior of a semiflexible polymer [36–39] to determine the free energy of the chain throughout the looping process. We use this free-energy treatment to formulate the looping rate as a mean first-passage time process. Our model aims to incorporate the interplay between HP1α binding and the methyltransferase SuVar3-9 function, providing a sufficiently detailed treatment that is amenable to experimental assessment through perturbation to the HP1α and SuVar3-9 levels. We find that the relative timescales of the kinetics of the methyltransferase and the dynamics of transient looping dictate the extent of methyl spreading. Chromosomal dynamics are essential for the efficient spreading of methyl marks, especially for mid-range inter-chromosomal segment lengths. Our model illustrates that the re-establishment of the epigenetic code upon cell division may depend on the physical organization of the DNA polymer, a hypothesis which will be further explored in future work.

2. Results and discussion

Our theoretical model for loop-mediated methylation is constructed in three stages. First, we develop a theoretical model to describe the dynamics of looping and unlooping processes of a section of chromosomal DNA based on polymer physics arguments. Second, we use the looping kinetics as a basis for a model for loop-mediated methylation, which predicts the spreading of methyl marks along the chromosome via the stochastic processes of looping and methylation. Figure 1 shows a schematic representation of the kinetic processes involved in the conferral and removal of a methyl mark on a distal nucleosome from a marked nucleosome. Third, we develop a master equation treatment to predict the temporal evolution of the methylation distribution and the steady-state methylation profile.

2.1. DNA looping statistics and kinetics

Chromosomal DNA is organized into a structure that is dictated by DNA-associated proteins, including histones, CTCF, and HP1. This organization depends on the epigenetic state of the

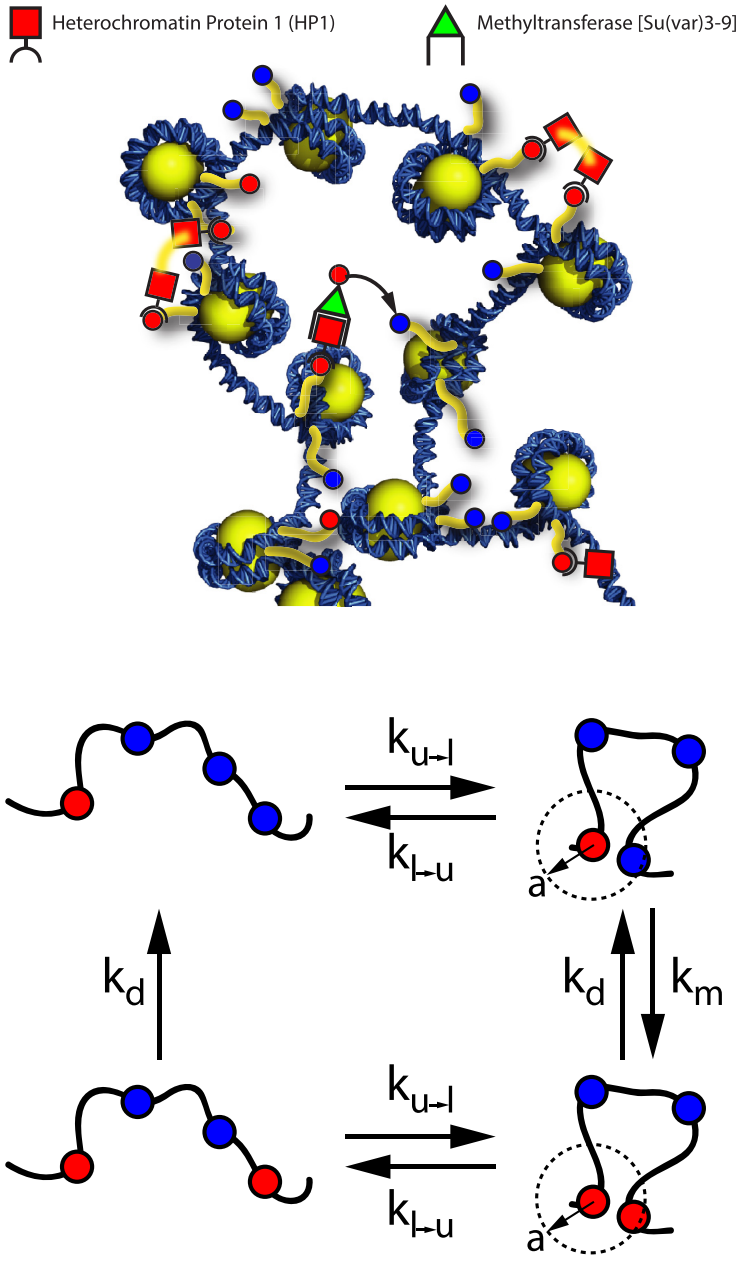

Figure 1. The top schematic depicts an array of nucleosomes and the interactions among methylation of H3K9, HP1α, and the methyltransferase SuVar3-9. The bottom schematic represents the kinetic processes that are involved in the conferral and removal of a methyl mark on a nucleosome via chromosomal looping and methyltransferase function. Each bead represents a nucleosome that is either methylated (red) or unmethylated (blue). The rate of looping $k_{u\to l}$ and rate of unlooping $k_{l\to u}$ for a chromosomal segment dictate events in which two genomically distant nucleosomes are within a distance a. Upon looping, a methyl mark is conferred to the distant site with rate k_m, and demethylation of the site occurs with rate k_d.

cell and the stage in the cell cycle. Our current work is inspired by observations of methylation spreading in undifferentiated stem cells [9]. Therefore, we assume the chromosomal DNA is uncondensed and able to dynamically adopt looped configurations that arise from thermal fluctuations that offset the local deformation free energy of the chain. The simplest description of such polymer behavior is the wormlike chain model, which describes an elastic chain subjected to thermal fluctuations [40, 41]. Although the local packaging of nucleosomal DNA may be better described as a fluctuating zig–zag polymer [42], our current aim is to identify the dominant physical effects that dictate the dynamic spreading of methyl marks, and future theoretical development will focus on more detailed descriptions of the chromosomal DNA enabled by our coarse-graining approaches [42–44].

The wormlike chain model describes the statistical behavior of a fluctuating elastic chain. The space curve $\vec{r}(s)$ defines the shape of the chain over the arclength parameter s, where s runs from 0 at one end to the chain length L at the opposite end. The bending deformation energy of the chain is given by

$$\beta E_{\text{bend}} = \frac{l_{\text{p}}}{2} \int_0^L \mathrm{d}s \left(\frac{\partial \vec{u}}{\partial s} \right)^2 , \tag{1}$$

where $\beta = 1/(k_{\text{B}}T)$, l_{p} is the persistence length of the chain, and $\vec{u} = \frac{\partial \vec{r}}{\partial s}$ is the chain tangent vector. The wormlike chain is assumed to be inextensible (i.e. $|\vec{u}| = \left| \frac{\partial \vec{r}}{\partial s} \right| = 1$ for all s), which is strictly enforced in our work.

The end-to-end distance distribution (i.e. the Green function for chain propagation) is formally determined as

$$\begin{aligned} &G(\vec{R}; L) \\ &= \int_{\vec{r}(0)=\vec{0}}^{\vec{r}(L)=\vec{R}} \mathcal{D}[\vec{r}(s)] \exp\left(-\beta E_{\text{bend}}\right) \prod_s \delta\left(|\vec{u}(s)| - 1\right), \end{aligned} \tag{2}$$

where $\int \mathcal{D}[\vec{r}(s)]$ indicates a path integral over all configurations $\vec{r}(s)$ that begin at the origin and end at position $\vec{r}(L) = \vec{R}$. The delta function constraint ensures inextensibility is not violated in the path integration. Our previous work [36–39] provides exact results for the Fourier–Laplace-transformed Green function $\hat{\tilde{G}}(\vec{k}; p)$ (i.e. Fourier transformed from $\vec{R}$ to $\vec{k}$ and Laplace transformed from $N = L/(2_{\text{p}})$ to p), given by

$$\hat{\tilde{G}}(\vec{k}; p) = \cfrac{1}{P_0 + \cfrac{a_1^2 K^2}{P_1 + \cfrac{a_2^2 K^2}{P_2 + \cfrac{a_3^2 K^2}{P_3 + \ldots}}}} \tag{3}$$

where $P_n = p + l(l+1)$, $K = 2l_{\text{p}}|\vec{k}|$, and the ellipses indicate an infinite continued fraction. Inversions of the Fourier and Laplace transforms are conducted using numerical approaches developed in detail in [39].

We define a loop radius a, which determines whether the polymer chain is in the unlooped ($|\vec{R}| > a$) or the looped ($|\vec{R}| \leq a$) state. In this work, we set this quantity to $a = 3.34\,\text{nm}$, which results in the near-neighbor nucleosomes being outside the loop radius for all values of inter-nucleosome spacing explored. Thus, inter-nucleosome communication occurs via looping events rather than direct spreading along the chain. The probability that the chain is in the looped state $P_{\text{l}}(a, L)$ is given by

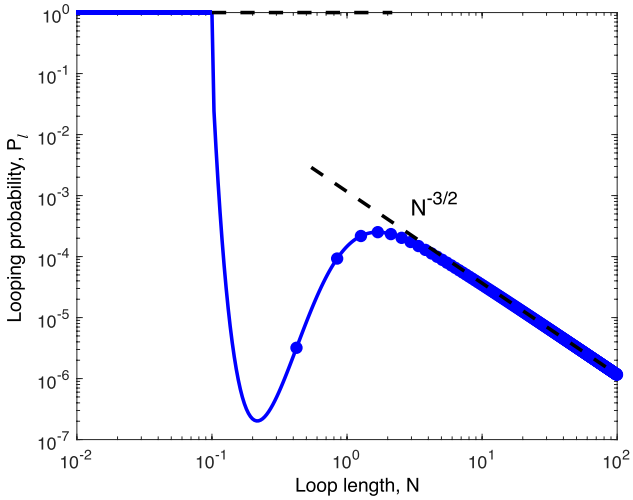

Figure 2. Looping probability as a function of polymer length $N = L/(2l_\mathrm{p})$ for a reaction radius $a/(2l_\mathrm{p}) = 0.094$ ($a = 3.34\,\mathrm{nm}$ and $l_\mathrm{p} = 17.68$ nm). Discrete points identify the segment lengths corresponding to a linker length of 45 basepairs between nucleosomes. Power-law scaling $N^{-3/2}$ demonstrates the asymptotic trend towards Gaussian-chain behavior as $N \to \infty$.

$$P_\mathrm{l}(a, L) = 4\pi \int_0^a \mathrm{d}R\, R^2 G(R; L). \tag{4}$$

The looping probability P_l is determined over a range of N, shown in figure 2. The looping probability is dictated by a balance between competing factors: the bending energy, which dominates at short length scales, and the conformational entropy, which dominates at long length scales. At intermediate length scales, the looping probability increases as the chain becomes more flexible. Hence, the looping probability decreases non-monotonically as the polymer length increases. In the limit of large N, the wormlike chain behaves like a flexible Gaussian chain, and the looping probability scales as $N^{-3/2}$, reflecting the entropic cost for looping a flexible chain in three dimensions. Since the looping probability P_l is very small ($P_\mathrm{l} < 0.0006$), nested loops with multiple internal loops are extremely rare. Thus, we assume that each looping event within a very long chain can be treated as a separate event that is decoupled from other loops that may form within the chain.

The looping probability P_l provides the equilibrium probability of finding the chain ends within a distance a. However, the dynamic transitions between the looped and unlooped states require a treatment of the stochastic motion of the chain biased by the underlying thermodynamic driving forces of chain bending energy and conformational entropy. In this work, we assume the motion of the chain ends is governed by a pseudo-equilibrium treatment in which the chain is able to instantaneously relax throughout the looping process. Based on general polymer physics models, the longest wavelength motion of the chain (i.e. relative motion of the chain ends) corresponds to the longest time scale of relaxation [45]. However, looping processes of very long polymer chains are not adequately predicted by the pseudo-equilibrium assumption [46, 47], and internal chain dynamics must be accounted for in the theory.

We determine the mean first-passage time for looping $t_{u\to l}$ (i.e. going from the unlooped state to the looped state) based on biased diffusion with the free energy $F = -k_{\mathrm{B}}T \log\left[R^2 G(R;L)\right]$. Based on our previous work [22, 23], we write the governing differential equation for $t_{u\to l}$ as

$$D\left(\frac{\partial^2 t_{u\to l}}{\partial R^2} + \frac{f}{k_{\mathrm{B}}T}\frac{\partial t_{u\to l}}{\partial R}\right) = -1 \tag{5}$$

and boundary conditions

$$t_{u\to l}(R = a) = 0 \tag{6}$$

$$\left.\frac{\partial t_{u\to l}}{\partial R}\right|_{R=L} = 0, \tag{7}$$

where D is the diffusion coefficient for the chain motion (to be discussed below), and the free energy F is used to determine the force $f = -\frac{\partial F}{\partial R} = k_{\mathrm{B}}T\frac{\partial \log\left(R^2 G\right)}{\partial R}$. Solving this differential equation results in the looping time $t_{u\to l}$ from a starting position R, and we find the looping time (or the unlooped lifetime) averaged over the starting position to be

$$\begin{aligned}\langle t_{u\to l}\rangle = {} & \frac{4\pi}{D(1-P_{\mathrm{l}})} \\ & \times \int_a^L \mathrm{d}R \int_a^R \mathrm{d}R' \int_{R'}^L \mathrm{d}R'' \frac{R^2 G(R;L) R'^2 G(R'';L)}{R'^2 G(R';L)}.\end{aligned} \tag{8}$$

We assume the looping kinetics are adequately captured by a Poisson process, and we define a looping rate as $k_{u\to l} = 1/\langle t_{u\to l}\rangle$. For simplicity, we construct the unlooping rate $k_{l\to u}$ (i.e. going from the looped state to the unlooped state) by ensuring the looping probability P_{l} is given by

$$P_{\mathrm{l}} = \frac{\langle t_{l\to u}\rangle}{\langle t_{l\to u}\rangle + \langle t_{u\to l}\rangle} = \frac{k_{u\to l}}{k_{l\to u} + k_{u\to l}}, \tag{9}$$

resulting in the expression

$$k_{l\to u} = k_{u\to l}\frac{1-P_{\mathrm{l}}}{P_{\mathrm{l}}}. \tag{10}$$

For our pseudo-equilibrium treatment of the looping kinetics, the diffusivity D is determined by the Stokes–Einstein relation $D = k_{\mathrm{B}}T/\xi$, where ξ is the drag coefficient on the chain. In this work, we assume D is an effective diffusivity that does not exhibit a strong chain-length dependence. This assumption is verified using Brownian dynamics simulations (discussed below).

Figure 3 shows the looped lifetime $\langle t_{l\to u}\rangle$ (top plot) and unlooped lifetime $\langle t_{u\to l}\rangle$ (bottom plot) versus the polymer length $N = L/(2l_{\mathrm{p}})$. These lifetimes are non-dimensionalized by the time $(2l_{\mathrm{p}})^2/D$, which defines the timescale for the chain end to diffuse a distance comparable to a Kuhn length $2l_{\mathrm{p}}$. The power-law scalings within figure 3 indicate the expected behaviors in the large-length limit as that of a Gaussian chain.

To validate our theoretical predictions for the unlooped lifetimes, we perform Brownian dynamics simulations of a wormlike chain. Based on our previous work [42–44], the dynamic behavior of a wormlike chain is efficiently captured using the discrete stretchable, shearable wormlike chain (dssWLC) model. The dssWLC model is defined by a set of beads numbered from 0 to M, with positions $\vec{r}_i$ and a unit tangent vector $\vec{u}_i$ attached to each bead. The energy function for a given chain configuration is given by [43]

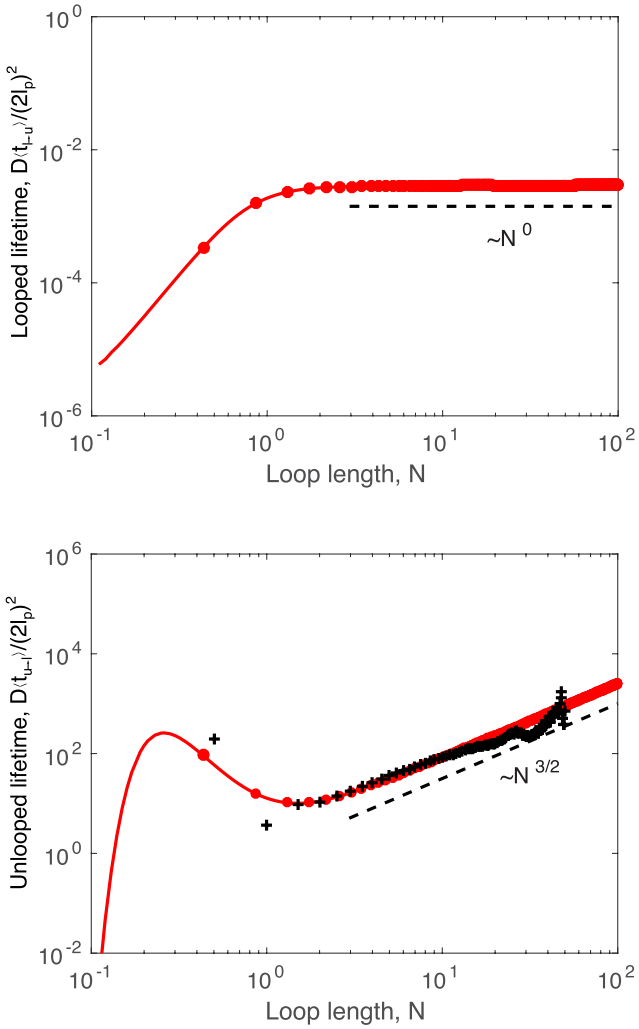

Figure 3. Looped lifetime $\langle t_{l\to u}\rangle$ (top plot) and unlooped lifetime $\langle t_{u\to l}\rangle$ (bottom plot) versus the polymer length $N = L/(2l_{\mathrm{p}})$. Discrete points (in red) identify our theoretical predictions for segment lengths corresponding to a linker length of 45 basepairs between nucleosomes. The black points in the bottom plot give the unlooped lifetime calculated from simulation data.

$$\beta E(\{\vec{R}_i,\vec{u}_i\}) = \sum_{i=1}^{M}\Big[\frac{\epsilon_b}{2\Delta}|\vec{u}_i-\vec{u}_{i-1}-\eta\vec{R}_i^{\perp}|^2 + \frac{\epsilon_{\parallel}}{2\Delta}(\vec{R}_i\cdot\vec{u}_{i-1}-\Delta\gamma)^2+\frac{\epsilon_{\perp}}{2\Delta}|\vec{R}_i^{\perp}|^2\Big] \tag{11}$$

where $\beta = 1/(k_{\mathrm{B}}T)$, k_{B} is the Boltzmann constant, $\vec{R}_i = \vec{r}_i - \vec{r}_{i-1}$ and $\vec{R}_i^{\perp} = \vec{R}_i - (\vec{R}_i\cdot\vec{u}_{i-1})\vec{u}_{i-1}$. Each segment of this discrete model represents a continuous polymer contour length of Δ. The model parameters include the bend modulus ϵ_b, stretch modulus $\epsilon_{\parallel}$, shear modulus $\epsilon_{\perp}$, fractional ground-state length γ, and bend-shear coupling η. These parameters can be found

for a wormlike chain with persistence length ℓ_p at any discretization length Δ, as described in our previous work [43].

We perform simulations of a dssWLC with a total length $N = 50$ and discretization length $\Delta = 0.5$ (i.e. the chain is composed of $M = 100$ beads). The initial condition is equilibrated using Monte Carlo simulations, and a Brownian dynamics simulation is performed until all sets of beads form a looped configuration (with a separation distance $a/(2l_p) = 0.094$). The recorded time is averaged to determine the unlooped lifetime for each set of inter-bead spacing, resulting in a simulation prediction for the unlooped lifetime versus chain length N. The results from our simulations are included as crosses in the bottom plot of figure 3. These results exhibit the characteristic scaling of $\langle t_{u\to l}\rangle \sim N^{3/2}$ for $N \gg 1$, substantiating the formulation of the unlooped lifetime based on the first-passage time process for a wormlike chain.

2.2. Loop-mediated methylation

We develop a model for the spreading of epigenetic marks along chromosomal DNA. In this work, we focus on the methylation of H3K9, but our model is amenable to other epigenetic modifications that involve spatial coordination of DNA loci. Furthermore, our treatment of DNA looping and reaction kinetics is relevant to the study of protein translocation along DNA via a facilitated diffusion mechanism [48–50]. Our model for methyl spreading incorporates several basic kinetic events that are involved in the spreading process.

To mimic the presence of HP1α and its subsequent cooperative binding of methyltransferase (i.e. SuVar3-9), nucleosomes can acquire a methyl mark by coming within a distance a of a genomically distant nucleosome to which HP1α is bound. However, a nucleosome is assumed to be incapable of self-methylation. As a result, the polymer must form a loop, with looping rate $k_{u\to l}$ and unlooping rate $k_{l\to u}$ (determined in the previous section), in order for a mark to be conferred. Once two nucleosomes are looped (i.e. within a distance a), a methyl mark can spread with a rate of methylation $k_m = k_m^{(0)} f$, where f is the probability that HP1α is bound to the site and $k_m^{(0)}$ represents the rate of methyltransferase activity. HP1α binding depends on whether the nucleosome is methylated or unmethylated, which is discussed further below. The methyltransferase rate $k_m^{(0)}$ depends on the amount of SuVar3-9 present in the cell and the strength of interaction between SuVar3-9 and the chromoshadow domain of a bound HP1α. We combine these factors into the rate constant $k_m^{(0)}$, and further experimental and theoretical work is necessary to develop a more detailed treatment. Finally, a methyl mark is removed from a nucleosome site with a rate of demethylation k_d. Demethylation may occur through a number of possible mechanisms, such as nucleosome turnover and chemical demethylation, and each of these mechanisms may proceed with a different rate constant. For simplicity, we include one effective rate constant for all demethylation in our model.

We now proceed to describe an effective methylation rate between distant nucleosomes that captures the underlying looping fluctuations. We assume at time $t = 0$ that the nucleosome transitions to the demethylated state and that the polymer begins in either the looped or unlooped state based on its equilibrium statistics (with probabilities P_l and $1 - P_l$, respectively). At some later time t, a methyl mark will be conferred to the nucleosome from a genomically distant site via an arbitrary number of looping and unlooping events.

We define the effective methylation waiting-time distribution $w_m^{\text{eff}}(t)$ such that $w_m^{\text{eff}}(t)\mathrm{d}t$ gives the probability that a methyl mark is conferred to the nucleosome between t and $t + \mathrm{d}t$. For ease of calculation, we adopt the Laplace transform from t to s, resulting in the Laplace-transformed waiting time distribution

$$\tilde{w}_m^{\text{eff}}(s) = \frac{k_m}{s + k_m + k_{l\to u}} \left[P_1 \frac{1}{1 - \frac{k_{l\to u}}{s+k_m+k_{l\to u}} \frac{k_{u\to l}}{s+k_{u\to l}}} + (1 - P_1) \frac{\frac{k_{u\to l}}{s+k_{u\to l}}}{1 - \frac{k_{l\to u}}{s+k_m+k_{l\to u}} \frac{k_{u\to l}}{s+k_{u\to l}}} \right]. \tag{12}$$

We include a detailed derivation of equation (12) in the appendix of this manuscript. We determine the effective methylation time $\langle t_m^{\text{eff}} \rangle$ using the property

$$\begin{aligned} \langle t_m^{\text{eff}} \rangle &= \int_0^\infty \mathrm{d}t\, t w_m^{\text{eff}}(t) = -\lim_{s\to 0} \frac{\mathrm{d}\tilde{w}_m^{\text{eff}}(s)}{\mathrm{d}s} \\ &= \frac{1}{k_m P_1} + \frac{1 - P_1}{k_{u\to l}}, \end{aligned} \tag{13}$$

and we define the effective methylation rate constant k_m^{eff} as

$$k_m^{\text{eff}} = k_m^{(0)} f P_1 \frac{1}{1 + P_1(1 - P_1)\frac{k_m^{(0)} f}{k_{u\to l}}}, \tag{14}$$

where we explicitly write $k_m = k_m^{(0)} f$. Notably, the condition $k_{u\to l} \gg k_m$ (looping is much faster than methylation) results in an effective methylation rate $k_m^{\text{eff}} \to k_m^{(0)} f P_1$, giving a rate constant weighted by the equilibrium looping probability P_1. Finite looping kinetics will always reduce the rate from this limit, and we define the efficiency factor

$$\eta = \frac{1}{1 + P_1(1 - P_1)\frac{k_m^{(0)} f}{k_{u\to l}}}, \tag{15}$$

such that $k_m^{\text{eff}} = k_m^{(0)} f P_1 \eta$. We define the dimensionless parameter $\alpha_1 = k_m^{(0)} (2l_p)^2 / D$ as the rate of methylation relative to the characteristic time scale of looping.

Figure 4 shows the effective methylation rate versus the chain length N for values of $\alpha_1 = 10^1$ (blue), 10^2, 10^3, and 10^4 (red) and the fraction of HP1α bound $f = 1$. The limit of $\alpha_1 \to 0$ coincides with the looping rate being much faster than the methylation rate. This limit results in $k_m^{\text{eff}} = k_m P_1$, as shown by the dashed curve in figure 4. Finite values of α_1 result in a lower efficiency η, which suppresses the effective methylation rate. The power-law scalings for the Gaussian chain model result in the prediction $P_1\eta \sim N^{-2}$ and $\eta \sim N^{-1/2}$, as shown in the top and bottom plots in figure 4.

The demethylation rate k_d gives the rate of losing a methyl mark on the nucleosome through periodic turnover. This rate process applies to the methylated state whether the chain is looped or unlooped. We define the dimensionless parameter $\alpha_d = k_m^{(0)} / k_d$ as the rate of methylation relative to the rate of demethylation. We have now defined all of the rate processes depicted in figure 1 for the methylation and demethylation of a single nucleosome. In the next section, we demonstrate how these rate processes are incorporated into a general model for the spreading of methyl marks within nucleosomes in chromosomal DNA.

2.3. Time-dependent methylation profile

Our kinetic model of looping, methylation, and demethylation forms the basis for modeling methylation spreading. In this work, our aim is to focus on the looping processes that arise in the methylation process. Thus, we neglect intermediate levels of methylation (i.e.

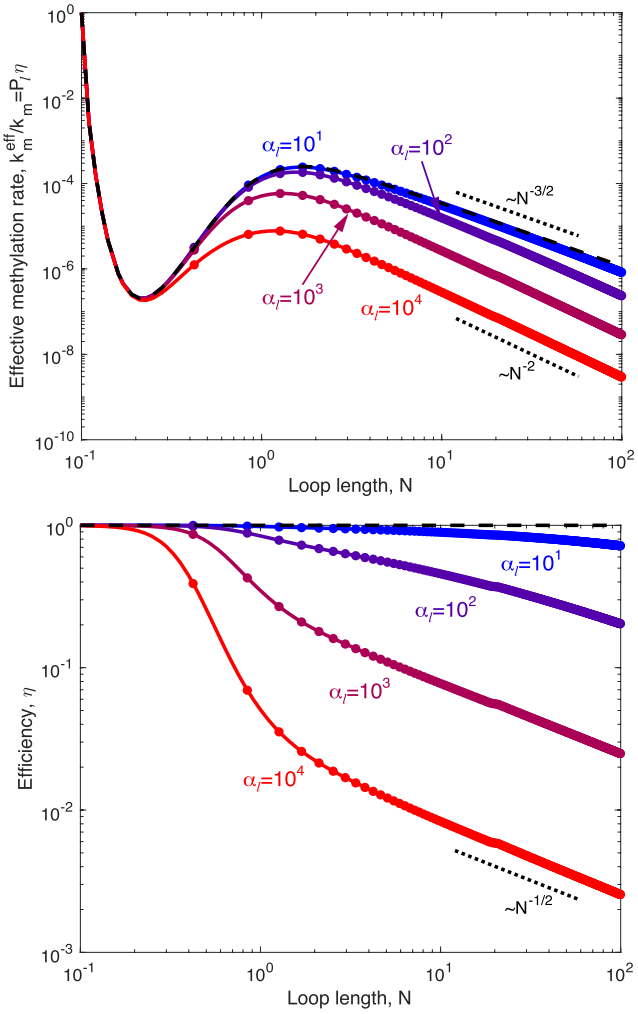

Figure 4. Top plot shows the effective methylation rate k_m^{eff}/k_m versus the loop length $N = L/(2l_{\text{p}})$ for $\alpha_{\text{l}} = k_m^{(0)}(2l_{\text{p}})^2/D = P_{\text{l}}\eta$ ranging from $\alpha_{\text{l}} = 10^1$ (blue) to $\alpha_{\text{l}} = 10^4$ (red) and the fraction of HP1α bound set to unity (i.e. $f = 1$). The dashed curve shows the behavior for $\eta = 1$ (i.e. $k_m^{\text{eff}} = k_m P_{\text{l}}$). Bottom plot shows the efficiency η for the same parameters as in the top plot. As in previous plots, discrete points identify a linker length of 45 basepairs between nucleosomes.

monomethylation and dimethylation). Furthermore, each nucleosome exists in either a methylated or unmethylated state without consideration of the methylated state of the two tails of the histone octamer. Our basic model presented here can be extended to include independent tails and the intermediate states, as is captured in previous efforts to model the spreading of related epigenetic marks [51].

Linker lengths connecting adjacent nucleosomes range from about 10 to 90 basepairs for different species and tissues [52, 53], and there is considerable heterogeneity in linker length even within a single genome [54]. Recent modeling work has shown that heterogeneously-spaced nucleosomes create a chromatin fiber whose looping properties match that of a single

wormlike chain with a reduced, effective persistence length, which is determined purely by the average nucleosome spacing [55]. Based on these results, we consider a string of nucleosomes separated by linker lengths of exactly 45 basepairs, the average linker length for our experimental system of interest [9]. We incorporate heterogeneity in nucleosome spacing implicitly by using the theoretically-predicted persistence length of 17.68 nm for a chain whose average linker length is 45 basepairs [55]. Future work will examine the extent to which explicit heterogeneity in linker lengths leads to greater local variation in the methylation profile.

We employ a master equation approach that describes the average methylation profile over time. This method captures the evolution of the profile but neglects instantaneous fluctuations in the local methylation as the spreading occurs. In future work, we will use a kinetic Monte Carlo simulation to capture instantaneous fluctuations in the methylation.

The average methylation of the ith nucleosome in the chain is defined by the probability $p_i(t)$. We assume methylation occurs by the kinetic mechanism defined in figure 1, where a nucleosome to which HP1α is bound must loop with an unmethylated nucleosome for the methyltransferase to confer methylation to the unmethylated nucleosome. We assume that demethylation is independent of the looped state of the nucleosome. Since looping is a rare event, we neglect nested loops in our consideration of the looping between any two nucleosomes. In other words, all looping events are considered to be independent of all other looping events.

With these assumptions, the probability distribution $p_i(t)$ is governed by the master equation

$$\begin{aligned}\frac{\mathrm{d}p_i}{\mathrm{d}t} &= \sum_{j\neq i} k^{\mathrm{eff},m}_{m_{ij}}(1-p_i)\,p_j \\ &\quad + \sum_{j\neq i} k^{\mathrm{eff},u}_{m_{ij}}(1-p_i)(1-p_j) \\ &\quad + k^{\mathrm{eff},n}_{m_i}(1-p_i) - k_d p_i. \end{aligned} \tag{16}$$

The methylation rate from an already methylated nucleosome $k^{\mathrm{eff},m}_{m_{ij}} = k^{\mathrm{eff}}_m(N_{ij}, f = f_m)$, and the methylation rate from an unmethylated nucleosome $k^{\mathrm{eff},u}_{m_{ij}} = k^{\mathrm{eff}}_m(N_{ij}, f = f_u)$, where N_{ij} is the number of Kuhn lengths between the ith and jth nucleosomes (i.e. $N_{ij} = L_{ij}/(2l_\mathrm{p})$). The HP1 binding fraction f_m is the average fraction of HP1α molecules bound to a methylated nucleosome, and f_u is the average fraction of HP1α molecules bound to an unmethylated nucleosome. Experimental measurements [9] exist that address the spreading of methylation near a chemically linked HP1α protein, dubbed a nucleation site. The methylation rate from the nucleation site $k^{\mathrm{eff},n}_{m_i} = k^{\mathrm{eff}}_m(N^n_i, f = 1)$, where N^n_i is the number of Kuhn lengths between the ith nucleosome and the nucleation site. Since the nucleation site contains a single chromoshadow domain of HP1α, we capture the strength of the HP1α content by setting $f = 1$ within $k^{\mathrm{eff},n}_{m_i}$.

The steady-state profile p^{ss}_i is determined by setting $\frac{\mathrm{d}p^{\mathrm{ss}}_i}{\mathrm{d}t} = 0$. The governing equation for p^{ss}_i is given by

$$\begin{aligned} 0 &= \sum_{j\neq i} k^{\mathrm{eff},m}_{m_{ij}}(1-p^{\mathrm{ss}}_i)\,p^{\mathrm{ss}}_j \\ &\quad + \sum_{j\neq i} k^{\mathrm{eff},u}_{m_{ij}}(1-p^{\mathrm{ss}}_i)(1-p^{\mathrm{ss}}_j) \\ &\quad + k^{\mathrm{eff},n}_{m_i}(1-p^{\mathrm{ss}}_i) - k_d p^{\mathrm{ss}}_i. \end{aligned} \tag{17}$$

To illustrate the general behavior of the steady-state profile, we consider the homogeneous solution $p_i^{ss} = p$ for homogeneous inter-nucleosome spacing in the absence of a nucleation site, which is governed by

$$0 = \alpha_d \kappa f_m p(1-p) + \alpha_d \kappa f_u (1-p)^2 - p, \tag{18}$$

where the connectivity factor $\kappa = \sum_{j \neq 0} P_{l_{ij}} \eta_{ij}$, and $\alpha_d = k_m^{(0)}/k_d$. This equation has two solutions, and the physically relevant solution is given by

$$\begin{aligned} p = & \frac{\sqrt{(\alpha_d \kappa f_m)^2 - 2\alpha_d \kappa (f_m - 2f_u) + 1}}{2\alpha_d \kappa (f_m - f_u)} \\ & + \frac{\alpha_d \kappa (f_m - 2f_u) - 1}{2\alpha_d \kappa (f_m - f_u)}. \end{aligned} \tag{19}$$

This homogeneous solution is valuable in assessing the general behavior of our model. In addition, the inhomogeneous solution p_i tends to the homogeneous solution p at distances sufficiently far from the nucleation site. Thus, the solution for equations (16) and (19) is found for a finite number of nucleosomes (200 total in this manuscript), and looping to nucleosomes outside the range is approximated by the methylation probability as $p_i \approx p$. We numerically verify that all our solutions are insensitive to the number of nucleosomes modeled.

The HP1α concentration C_{HP1} determines the values of the constants f_m and f_u based on the binding isotherm produced from experimental data [5]. Notably, the experimental measurements determine the binding of the *Schizosaccharomyces pombe* HP1 protein, Swi6, rather than mammalian HP1α. Further experimental data characterizing mammalian HP1 variants would be valuable for a more detailed development of such models for the spreading of epigenetic marks. Canzio *et al* measure the average fraction of Swi6 molecules bound to unmethylated mononucleosomes and to methylated mononucleosomes for various concentrations of HP1. Their results indicate that HP1 binds to both methylated and unmethylated nucleosomes but binds preferentially to methylated ones. We then use these experimental values of f_m and f_u as input to fit our model that is presented in [56]. In this model, we capture the equilibrium binding of HP1 to methylated and unmethylated single nucleosomes. Our statistical mechanics treatment captures the energy of binding to a methylated and unmethylated tail (ϵ_m and ϵ_u, respectively) and the cooperative HP1 interaction energy J when both tails have HP1 bound. Figure 5 shows the experimental measurements of HP1 binding to unmethylated (blue dots) and methylated (red dots) mononucleosomes versus the HP1 concentration C_{HP1}. We fit the experimental data to our binding model [56], resulting in a best-fit model for binding energy to a methylated nucleosome relative to an unmethylated nucleosome $\epsilon_m - \epsilon_u = 1.53\, k_{\mathrm{B}}T$ (positive is favorable) and a HP1 interaction energy $J = 3.92\, k_{\mathrm{B}}T$.

These measurements of f_m and f_u are for mononucleosomes and may not be accurate for nucleosomes that are connected in a chain. In fact, it is likely that the presence of several methylated nucleosomes in spatial proximity has a cooperative effect, leading to an enhancement in the binding of HP1α as exhibited in binding assays to dinucleosomes [5]. For now, we use the direct experimental measurements of f_m and f_u and neglect this cooperativity, though such an effect will be addressed in future work on methylation in chromosomal DNA that exhibits heterochromatin and euchromatin segregation.

Figure 6 provides results for the steady-state probability of methylation. The top plot of figure 6 shows predictions of the 'phase diagram' for methylation spreading based on the homogeneous solution. The bottom plot shows the probability of methylation as a function of C_{HP1} for the five values of α_d identified by horizontal lines in the top plot. The smooth transition of the fraction methylated p with increasing HP1 concentration C_{HP1} indicates an onset of methylation.

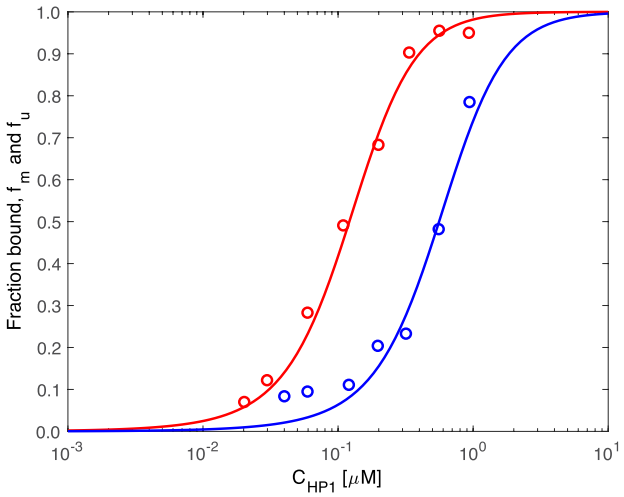

Figure 5. Fraction of HP1 bound to unmethylated (f_u, blue) and tri-methylated (f_m, red) nucleosomes. The dots provide experimental measurements for the fraction bound for Swi6 (an HP1 analog in *S. pombe*) [5], and the curves show our binding model [56]. The model that gives the best fit to the experimental data predicts a favorable binding energy to a methylated nucleosome relative to an unmethylated nucleosome to be $\epsilon_m - \epsilon_u = 1.53\, k_B T$ and a HP1 interaction energy $J = 3.92\, k_B T$.

At low HP1 concentrations, methylation is localized and unable to spread over the entire chain. In contrast, at high HP1 concentrations, there are sufficient HP1α molecules bound to proximal nucleosomes for transient looping to enable unchecked spreading along the chain. Since HP1α binds to unmethylated nucleosomes, our model predicts a basal level of methylation that occurs from transient looping events with unmethylated nucleosomes with HP1α bound.

The methylation spreading observed in experiments spans only about 10 kilobases [9], and at lengthscales this small, the looping kinetics are relatively fast, as shown in figure 4. Therefore, it is reasonable for us to assume maximal efficiency for all loop lengths (i.e. $\eta = 1$) and to approximate the effective methylation rate as the absolute methylation rate weighted by the equilibrium looping probability (i.e. $k_m^{\text{eff}} = k_m P_l$). Under this approximation, we allow $\alpha_l \to 0$ in figure 6 and show the effects of α_d and the concentration of HP1 on the probability of methylation. Were α_l to take a higher value, the efficiency and effective methylation rate would decrease, resulting in a larger region of low methylation probability (shown in black) in the 'phase diagram'. Non-negligible values of the methylation probability could still be achieved but would require a higher value of α_d and/or a higher concentration of HP1.

The extent of methyl spreading depends on the combination of parameter values: α_d, α_l, and C_{HP1}. In some regions of the phase diagram, the probability of methylation is essentially zero, indicating that methyl marks are incapable of spreading in that parameter regime. In contrast, in other regions of the phase diagram, the probability of methylation takes a constant, non-zero value. In these parameter regimes, methyl marks can spread indefinitely along the polymer. Because we assume the chromosome is uncondensed, there are no structural components to prevent contact between distal parts of the chromosome, and eventually marks could spread along the entire chain through a series of looping events. Without higher order structural organization, the marks cannot be confined to a particular domain. Upcoming work will explore the important role that both local and global chromatin organization play in establishing and maintaining domains of methylation.

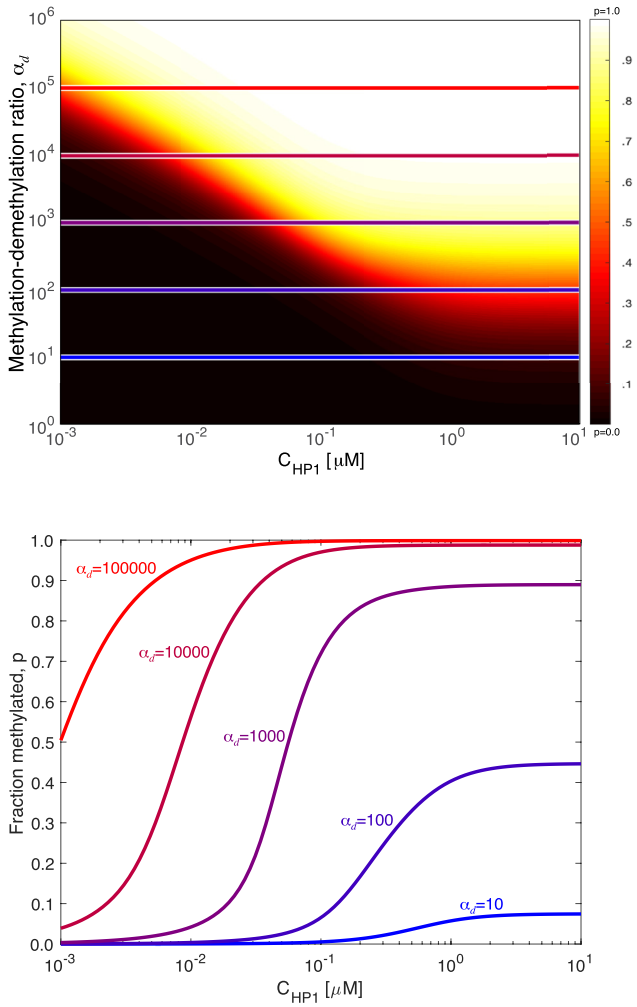

Figure 6. Probability of methylation for nucleosomes in a homogeneous chain with a linker length of 45 basepairs. The top plot shows the 'phase diagram' for a persistence length of 17.68 nm. The bottom plot shows the probability of methylation for the five values of α_d identified by the horizontal lines in the top plot.

To gain a better sense of which regime in our model most closely aligns with *in vivo* conditions, we proceed to consider the order of magnitude of our model parameters. Estimates suggest that the concentration of HP1α bound to chromatin is on the order of 100 μM *in vivo* [57]. A thermodynamic model of HP1 binding to chromatin, fit to experimental data [5], implies that the free concentration of HP1 is much lower than the bound concentration and may lie between 10^{-2} μM and 1 μM [56]. Experimental FCS measurements of GFP-tagged proteins coupled with APD-imaging support this estimate, reporting a concentration of 0.06 μM for HP1α in the cytoplasm of mouse fibroblasts [58].

It is difficult to estimate the order of magnitude of α_d and α_1 for an *in vivo* system given the uncertainty around the bare methylation rate, $k_m^{(0)}$. Mass spectrometry experiments have been used to observe histone methylation dynamics in HeLa cells, and fitting a simple mass-action model to this data indicates that the order of the methylation rate may be between 10^{-2}/d and

1/d [59]. *In vitro* experiments of the kinetics of the murine H3K9 methyltransferase G9a find that methylation occurs on the order of hours [60].

Single-molecule optical tracking experiments in mammalian cells find that the diffusion coefficient of genetic loci is roughly on the order of 1 μm^2 min^{-1} [61]. Based on these estimates for the methylation rate and diffusion coefficient, α_1 would be on the order of 10^{-8}–10^{-5}. This approximate range of values corresponds to a regime in which looping dynamics are much faster than methylation dynamics.

Histone labeling experiments in Drosophila cells show that nucleosomes in active genes turn over approximately once every 1–2 h [62], which would put α_d (i.e. k_m/k_d) on the order of 10^{-3} to 10^0. However, experiments of the dynamics of H3K79 methylation in mouse embryonic stem cells reveal that turnover dynamics vary across substrates, suggesting that the turnover rate is different at different genomic locations [51]. This result adds to the uncertainty in estimating α_d. Furthermore, a simple yet foundational model of methyl spreading indicates that the relative rate of methylation is around 1 to 1.5. According to this model, a value of 1.5 for k_m/k_d is the best fit for experimental H3K9 spreading data in mouse ES cells [9, 10]. In our model, we find that relative enrichment $p_i^{ss}/p_i^{ss(0)}$ is fairly insensitive to α_d, since α_d proportionately affects both p_i^{ss} and $p_i^{ss(0)}$. Interpretation of the absolute value of the fraction methylation is not possible from the ChIP-seq data [9], and further experimental analyses would be valuable to fully determine the absolute fraction methylation. This would allow a more extensive determination of model parameters, including α_d.

3. Conclusions

In this work, we propose a physical mechanism for the spreading of methylation due to transient chromosomal looping. This theory extends the foundational work of Hodges and Crabtree [10], which addresses how chromosomal contacts would facilitate the spreading of methylation marks to distal chromosomal segments based on the probability of these contacts. Our treatment aims to address the influence of chromosomal dynamics on the spreading, providing a basic picture of the competition between the methyltransferase enzymatic rate and the chromosomal dynamics. Our theory for the effective methylation rate also provides a major advantage for simulation efforts, in that it reproduces the results of more detailed simulations for a fraction of the computational cost.

Our model shows that the looping probability acts as an upper bound on the effective methylation rate, with maximum rates only possible in the limit that looping dynamics are instantaneous (i.e. the DNA can rearrange its configuration much faster than a methyl mark can be conferred). Otherwise, the characteristic timescale of looping, which is extremely slow based on *in vivo* measurements, is predicted to result in low methylation efficiency and effective methylation rate. For a fixed timescale of looping, there are two regimes of spreading behavior. A low relative rate of methylation α_d and HP1α concentration C_{HP1} restricts methylation spreading, whereas a high relative rate of methylation allows methylation to spread along the entire chain. Regardless of the timescale of methylation, the predicted length-scale dependence of the effective methylation rate suggests that looping will always be a limiting factor for effective methylation for large inter-chromosomal segment lengths. This implies that the distal communication between chromosomal loci is essentially dictated by the initial organization, which is unable to fully explore the nuclear environment. Thus, the coordination of distal segments via dynamic rearrangement of the chromosome is not a viable mechanism for robust conferral of methyl marks.

Epigenetic modifications occur along the entire chromosome, and a better understanding of the spreading behavior at longer lengthscales is required. Furthermore, once methylation spreads and the epigenetic pattern is established, it must be maintained over generations in order to ensure continuity of cellular identity and behavior. Ongoing work seeks to address these topics. Given that epigenetic methylation and chromatin condensation are connected through the oligomerization of HP1, we are currently extending our model of loop-mediated methylation to incorporate the interplay of these two processes and to study their combined effect on the methylation profile and chromatin structure.

Acknowledgments

This manuscript is dedicated to the memory of Jörg Langowski. The field of physical modeling of chromosomal DNA has lost an inspirational researcher and thought leader, and Jörg's boundless energy and enthusiasm will be greatly missed. We are grateful to Courtney Hodges, Emma Chory, Gerald Crabtree, Quinn MacPherson, and Deepti Kannan for helpful discussions. Financial support for this work is provided by the National Science Foundation, Physics of Living Systems Program (PHY-1707751), and SS acknowledges funding support from the NSF Graduate Research Fellowship program.

Appendix. Derivation of equation (12)

We define $w_{i\to j}(t)$ as the waiting time distribution for the polymer to transition from state i to state j, resulting in the expressions

$$\begin{aligned} w_{l\to m}(t) &= k_m \exp[-(k_m + k_{l\to u})t], \\ w_{l\to u}(t) &= k_{l\to u} \exp[-(k_m + k_{l\to u})t], \\ w_{u\to l}(t) &= k_{u\to l} \exp[-k_{l\to u}t]. \end{aligned} \tag{A.1}$$

We take the Laplace transform of $w_{i\to j}(t)$ to get $\tilde{w}_{i\to j}(s)$, given by

$$\begin{aligned} \tilde{w}_{l\to m}(s) &= \frac{k_m}{s + k_m + k_{l\to u}}, \\ \tilde{w}_{l\to u}(s) &= \frac{k_{l\to u}}{s + k_m + k_{l\to u}}, \\ \tilde{w}_{u\to l}(s) &= \frac{k_{u\to l}}{s + k_{u\to l}}. \end{aligned} \tag{A.2}$$

Next, we find the overall waiting time distribution for going from the looped state to the methylated state $W_{l\to m}(t)$. In doing so, we must account for the infinite number of stochastic looping and unlooping events that might occur before a methyl mark is conferred. Therefore, we take the convolution of the real-space, single-event waiting time distributions and sum the number of cycles through the unlooped state to infinity, leading to

$$\begin{aligned} W_{l\to m}(t) = &\sum_{n=0,\,\text{even}}^{\infty} \int_0^t \mathrm{d}t_n \int_0^{t_n} \mathrm{d}t_{n-1} \cdots \int_0^{t_2} \mathrm{d}t_1 w_{l\to m}(t - t_n) \cdots \\ &w_{u\to l}(t_{j+1} - t_j) w_{l\to u}(t_j - t_{j-1}) \cdots w_{u\to l}(t_2 - t_1) w_{l\to u}(t_1) \\ = &\sum_{n=0,\,\text{even}}^{\infty} w_{l\to m}(t) * [w_{u\to l}(t) * w_{l\to u}(t)]^{n/2}. \end{aligned} \tag{A.3}$$

In Laplace space, the convolution results in a product of single-event waiting time distributions, allowing us to solve for $\tilde{W}_{l\to m}(s)$ as

$$\begin{aligned}\tilde{W}_{l\to m}(s) &= \sum_{n=0,\,\text{even}}^{\infty} \tilde{w}_{l\to m}(s)[\tilde{w}_{u\to l}(s)\tilde{w}_{l\to u}(s)]^{n/2} \\ &= \frac{\tilde{w}_{l\to m}(s)}{1-\tilde{w}_{u\to l}(s)\tilde{w}_{l\to u}(s)} \\ &= \frac{k_m(s+k_{u\to l})}{s^2+s(k_m+k_{l\to u}+k_{u\to l})+k_m k_{u\to l}}.\end{aligned} \tag{A.4}$$

Using the same technique, we find $W_{u\to m}(t)$ and $\tilde{W}_{u\to m}(s)$.

$$\begin{aligned}W_{u\to m}(t) &= \sum_{n=1,\,\text{odd}}^{\infty} \int_0^t \mathrm{d}t_n \int_0^{t_{n-1}} \mathrm{d}t_{n-1}\cdots\int_0^{t_1} \mathrm{d}t_1 w_{l\to m}(t-t_n)\cdots \\ &\quad w_{u\to l}(t_{j+1}-t_j)w_{l\to u}(t_j-t_{j-1})\cdots w_{u\to l}(t_1) \\ &= \sum_{n=1,\,\text{odd}}^{\infty} w_{l\to m}(t) * [w_{u\to l}(t) * w_{l\to u}(t)]^{(n-1)/2} * w_{u\to l}(t),\end{aligned} \tag{A.5}$$

which results in the Laplace-transformed waiting time distribution

$$\begin{aligned}\tilde{W}_{u\to m}(s) &= \sum_{n=1,\,\text{odd}}^{\infty} \tilde{w}_{l\to m}(s)[\tilde{w}_{u\to l}(s)\tilde{w}_{l\to u}(s)]^{(n-1)/2}\tilde{w}_{u\to l}(s) \\ &= \frac{\tilde{w}_{l\to m}(s)\tilde{w}_{u\to l}(s)}{1-\tilde{w}_{u\to l}(s)\tilde{w}_{l\to u}(s)} \\ &= \frac{k_m k_{u\to l}}{s^2+s(k_m+k_{l\to u}+k_{u\to l})+k_m k_{u\to l}}.\end{aligned} \tag{A.6}$$

The total effective waiting time distribution for the conferral of a methyl mark $\tilde{w}_m^{\text{eff}}(s)$ is given by the following equation:

$$\begin{aligned}\tilde{w}_m^{\text{eff}}(s) &= P_1\tilde{W}_{l\to m}(s) + (1-P_1)\tilde{W}_{u\to m}(s) \\ &= P_1\frac{k_m(s+k_{u\to l})}{s^2+s(k_m+k_{l\to u}+k_{u\to l})+k_m k_{u\to l}} + (1-P_1)\frac{k_m k_{u\to l}}{s^2+s(k_m+k_{l\to u}+k_{u\to l})+k_m k_{u\to l}} \\ &= \frac{k_m}{s+k_m+k_{l\to u}}\left[P_1\frac{1}{1-\frac{k_{l\to u}}{s+k_m+k_{l\to u}}\frac{k_{u\to l}}{s+k_{u\to l}}} + (1-P_1)\frac{\frac{k_{u\to l}}{s+k_{u\to l}}}{1-\frac{k_{l\to u}}{s+k_m+k_{l\to u}}\frac{k_{u\to l}}{s+k_{u\to l}}}\right],\end{aligned} \tag{A.7}$$

which provides the basis for equation (12).

ORCID iDs

Sarah H Sandholtz1 https://orcid.org/0000-0001-6605-4931
Bruno G Beltran https://orcid.org/0000-0003-2931-5412
Andrew J Spakowitz https://orcid.org/0000-0002-0585-1942

References

[1] Verschure P J, Van Der Kraan I, De Leeuw W, Van Der Vlag J, Carpenter A E, Belmont A S and Van Driel R 2005 *Mol. Cell. Biol.* **25** 4552–64
[2] Bannister A, Zegerman P, Partridge J, Miska E, Thomas J, Allshire R and Kouzarides T 2001 *Nature* **410** 120–4
[3] Lachner M, O'Carroll D, Rea S, Mechtler K and Jenuwein T 2001 *Nature* **410** 116–20
[4] Nakayama J, Rice J, Strahl B, Allis C and Grewal S 2001 *Science* **292** 110–3
[5] Canzio D, Chang E, Shankar S, Kuchenbecker K, Simon M, Madhani H, Narlikar G and Al-Sady B 2011 *Mol. Cell* **41** 67–81
[6] Fritsch L, Robin P, Mathieu J, Souidi M, Hinaux H, Rougeulle C, Harel-Bellan A, Ameyar-Zazoua M and Ait-Si-Ali S 2010 *Mol. Cell* **37** 46–56
[7] Peters A *et al* 2003 *Mol. Cell* **12** 1577–89
[8] Rea S *et al* 2000 *Nature* **406** 593–9
[9] Hathaway N A, Bell O, Hodges C, Miller E L, Neel D S and Crabtree G R 2012 *Cell* **149** 1447–60
[10] Hodges C and Crabtree G R 2012 *Proc. Natl Acad. Sci.* **109** 13296–301
[11] Erdel F and Greene E 2016 *Proc. Natl Acad. Sci.* **113** E4180–9
[12] Dodd I, Micheelsen M, Sneppen K and Thon G 2007 *Cell* **129** 813–22
[13] Micheelsen M, Mitarai N, Sneppen K and Dodd I 2010 *Phys. Biol.* **7** 026010
[14] Jost D and Vaillant C 2018 *Nucl. Acids Res.* **46** 2252–64
[15] Michieletto D, Orlandini E and Marenduzzo D 2016 *Phys. Rev.* X **6** 041047
[16] Weber S, Spakowitz A and Theriot J 2010 *Phys. Rev. Lett.* **104** 238102
[17] Weber S, Theriot J and Spakowitz A 2010 *Phys. Rev.* E **82** 011913
[18] Weber S C, Spakowitz A J and Theriot J A 2012 *Proc. Natl Acad. Sci.* **109** 7338–43
[19] Weber S C, Thompson M A, Moerner W E, Spakowitz A J and Theriot J A 2012 *Biophys. J.* **102** 2443–50
[20] Lampo T J, Kuwada N J, Wiggins P A and Spakowitz A J 2015 *Biophys. J.* **108** 146–53
[21] Lampo T J, Kennard A S and Spakowitz A J 2016 *Biophys. J.* **110** 338–47
[22] Chen Y J, Johnson S, Mulligan P, Spakowitz A J and Phillips R 2014 *Proc. Natl Acad. Sci.* **111** 17396–401
[23] Mulligan P J, Chen Y J, Phillips R and Spakowitz A J 2015 *Biophys. J.* **109** 618–29
[24] Dekker J, Rippe K, Dekker M and Kleckner N 2002 *Science* **295** 1306–11
[25] Rao S S *et al* 2014 *Cell* **159** 1665–80
[26] Le T, Imakaev M V, Mirny L A and Laub M T 2013 *Science* **342** 731–4
[27] Barbieri M, Chotalia M, Fraser J, Lavitas L M, Dostie J, Pombo A and Nicodemi M 2012 *Proc. Natl Acad. Sci.* **109** 1204799109
[28] Jost D, Carrivain P, Cavalli G and Vaillant C 2014 *Nucl. Acids Res.* **42** 9553–61
[29] Chiariello A M, Annunziatella C, Bianco S, Esposito A and Nicodemi M 2016 *Sci. Rep.* **6** 29775
[30] Di Pierro M, Cheng R R, Aiden E L, Wolynes P G and Onuchic J N 2017 *Proc. Natl Acad. Sci.* **114** 201714980
[31] Nuebler J, Fudenberg G, Imakaev M, Abdennur N and Mirny L A 2018 *Proc. Natl Acad. Sci.* **115** E6697–706
[32] MacPherson Q, Beltran B and Spakowitz A J 2018 *Proc. Natl Acad. Sci.* **115** 12739–44
[33] Rosa A and Everaers R 2008 *PLoS Comput. Biol.* **4** e1000153
[34] Rosa A, Becker N B and Everaers R 2010 *Biophys. J.* **98** 2410–9
[35] Sullivan J M O, Hendy M, Pichugina T, Wake G and Langowski J 2013 *Nucleus* **4** 390–8
[36] Spakowitz A J and Wang Z G 2004 *Macromolecules* **37** 5814–23
[37] Spakowitz A J and Wang Z G 2005 *Phys. Rev.* E **72** 041802
[38] Spakowitz A J 2006 *Europhys. Lett.* **73** 684
[39] Mehraeen S, Sudhanshu B, Koslover E F and Spakowitz A J 2008 *Phys. Rev.* E **77** 061803
[40] Kratky O and Porod G 1949 *Recueil Travaux Chimiques Pays-Bas* **68** 1106–22
[41] Saito N, Takahashi K and Yunoki Y 1967 *J. Phys. Soc. Japan* **22** 219
[42] Koslover E F and Spakowitz A J 2013 *Macromolecules* **46** 2003–14
[43] Koslover E F and Spakowitz A J 2013 *Soft Matter* **29** 7016–27
[44] Koslover E F and Spakowitz A J 2014 *Phys. Rev.* E **90** 013304
[45] Doi M and Edwards S F 1986 *The Theory of Polymer Dynamics* (Oxford: Oxford University Press)
[46] Wilemski G and Fixman M 1974 *J. Chem. Phys.* **60** 866–77

[47] Wilemski G and Fixman M 1974 *J. Chem. Phys.* **60** 878–90
[48] Díaz de La Rosa M A, Koslover E F, Mulligan P J and Spakowitz A J 2010 *Biophys. J.* **98** 2943–53
[49] Koslover E F, Díaz de la Rosa M A and Spakowitz A J 2011 *Biophys. J.* **101** 856–65
[50] Koslover E F, de la Rosa M A D and Spakowitz A J 2017 *J. Phys. A: Math. Theor.* **50** 074005
[51] Chory E J, Calarco J P, Hathaway N A, Bell O, Neel D S and Crabtree G R 2019 *Mol. Cell* **73** 61–72
[52] Givens R M, Lai W K M, Rizzo J M, Bard J E, Mieczkowski P A, Leatherwood J, Huberman J A and Buck M J 2012 *Nucl. Acids Res.* **40** 7176–89
[53] Spadafora C, Bellard M, Compton J and Chambon P 1976 *FEBS Lett.* **69** 281–5
[54] Holde K V 1988 *Chromatin* (New York: Springer)
[55] Beltran B, Kannan D, MacPherson Q and Spakowitz A 2019 (BioRxiv:708966)
[56] Mulligan P J, Koslover E F and Spakowitz A J 2015 *J. Phys.: Condens. Matter* **27** 064109
[57] Larson A G, Elnatan D, Keenen M M, Trnka M J, Johnston J B, Burlingame A L, Agard D A, Redding S and Narlikar G J 2017 *Nature* **547** 236–40
[58] Müller-Ott K *et al* 2014 *Mol. Syst. Biol.* **10** 746
[59] Zee B M, Levin R S, Xu B, LeRoy G, Wingreen N S and Garcia B A 2010 *J. Biol. Chem.* **285** 3341–50
[60] Patnaik D, Chin H G, Estève P O, Benner J, Jacobsen S E and Pradhan S 2004 *J. Biol. Chem.* **279** 53248–58
[61] Ghosh R P, Franklin J M, Draper W E, Shi Q, Beltran B, Spakowitz A J and Liphardt J T 2019 *Nat. Chem. Biol.* **15** 401–9
[62] Deal R B, Henikoff J G and Henikoff S 2010 *Science* **328** 1161–4